Tunable topological states in electron-doped HTT-Pt

Xiaoming Zhang,[1,2] Zhenhai Wang,[3] Mingwen Zhao,[1,*] and Feng Liu[2,4]
[1]*School of Physics and State Key Laboratory of Crystal Materials, Shandong University, Jinan, Shandong 250100, China*
[2]*Department of Materials Science and Engineering, University of Utah, Salt Lake City, Utah 84112, USA*
[3]*Peter Grünberg Research Center, Nanjing University of Posts and Telecommunications, Nanjing, Jiangsu 210003, China*
[4]*Collaborative Innovation Center of Quantum Matter, Beijing 100084, China*
(Received 30 November 2015; revised manuscript received 30 January 2016; published 1 April 2016)

Modulating topologically nontrivial states in trivial materials is of both scientific and technological interest. Using first-principles calculations, we propose a demonstration of electron-doping- (or gate-voltage-) induced multiple quantum states; namely, quantum spin Hall (QSH) and quantum anomalous Hall (QAH) states, in a single material of the organometallic framework (HTT-Pt) synthesized from triphenylene hexathiol molecules (HTT) and $PtCl_2$. At a low doping level, the trivial HTT-Pt converts to a QSH insulator protected by time-reversal symmetry (TRS). When the electronic doping concentration is further increased, TRS will be broken, making the HTT-Pt a QAH insulator. The band gaps of these topologically nontrivial states can be as large as 42.5 meV, suggesting robustness at high temperatures. The possibility of switching between the QSH and QAH states offers an intriguing platform for a different device paradigm by interfacing between QSH and QAH states.

DOI: 10.1103/PhysRevB.93.165401

I. INTRODUCTION

As the semiconductor industry continually shrinks the size of electronic components on silicon chips, the limits of the current technologies are reached due to increasingly smaller sizes being prevented by the fundamental laws of physics. Spintronics, with the advantage of high density and nonvolatility of data storage, fast data processing, and low-power consumption, has the potential to revolutionize the fabrication of electronic devices. Topological insulators (TIs) provide a promising class of spintronics materials because of their exotic dispersive bands and topologically nontrivial electronic states. TIs have a bulk energy gap, which is linked by gapless edge/surface states that facilitate quantized electronic conduction on the boundaries. The edge states in two-dimensional (2D) TIs with time-reversal symmetry (TRS), referred to as quantum spin Hall (QSH) states [1], can host spin currents with different spin orientations propagating in the helical edge states with opposite directions, where spin-orbit coupling (SOC) plays a role analogous to the external magnetic field in quantum Hall systems. QSH states can also give rise to so-called quantum anomalous Hall (QAH) states [2] when TRS is broken via inducing magnetism [3,4], where only one spin orientation propagates in the chiral edge states without a need for an external magnetic field.

The ability to control the electronic properties of a material by applying an external electric field is crucial for spintronics device applications. The electric field allows one to realize electron (or hole) doping and, consequently, to modulate the position of the Fermi level, resulting in unexpected physical phenomena. For example, as the electron-doping concentration in conventional solid-state field-effect transistors (FETs) reaches $\sim 10^{12}\,\mathrm{cm}^{-2}$, the electrons will behave as chiral particles [5–7]. A significant band-gap and inversion symmetry breakage can be achieved in bilayer graphene at an electron doping level of $5\times 10^{13}\,\mathrm{cm}^{-2}$ using a solid polymer electrolyte gate [8–10]. Recently, the doping level has been improved to $\sim 10^{14}\,\mathrm{cm}^{-2}$ for both electrons and holes by using high-capacitance gate insulators [11,12], at which magnetoresistance modulation [13] and surface superconductivity [14,15] were realized. Beside high-capacitance gate insulators, electron (or hole) doping can also be achieved by substituting atoms or hydrogen [16]. However, these strategies are quite limited in high-level electron (or hole) doping due to the lack of controllability and reversibility.

The regulation of Fermi level is often inevitable for detecting topologically nontrivial states in organic topological insulators (OTIs) [17–19], because in most cases the Fermi level is not exactly in the bulk band gap. For example, $Ni_3C_{12}S_{12}$ [20], which is a real 2D material predicted to be a member of OTIs, has the Fermi level located in the trivial band gap. Electron doping at a level of $2\times 10^{14}\,\mathrm{cm}^{-2}$ is needed to move the Fermi level to the topologically nontrivial band gap. Other OTIs, such as $Au_3C_{12}S_{12}$ [20], $Mn_3C_{12}S_{12}$ [21], $Ni_3(C_{18}H_{12}N_6)$ [22], and $Au_3(C_{18}H_{12}N_6)$ [23], also require doping electrons or holes with a magnitude of $10^{13}\,\mathrm{cm}^{-2}$. It is noteworthy that in these cases the doping mainly tunes the position of the Fermi level, but the electronic band topology of the OTIs remains intact. The transition from QSH to QAH states induced by electron (or hole) doping has never been reported for these OTIs.

Here, we demonstrate theoretically that electron doping cannot only regulate the Fermi level, but can also modify the electronic band topology of OTIs. Taking a real organometallic framework (HTT-Pt) as an example, we showed that at experimentally assessable doping levels, multiple transitions from a trivial insulator to a QSH insulator, and then to a QAH insulator, can take place in a single material. At a low doping concentration ($4.14\times 10^{13}\,\mathrm{cm}^{-2}$), the trivial HTT-Pt becomes a QSH insulator characterized by a nonzero Z_2 topological invariant, while at a higher doping level ($8.28\times 10^{13}\,\mathrm{cm}^{-2}$), it converts to a QAH insulator with a finite Chern number of $C = 1$, due to the TRS breakage and spontaneous spin polarization. More importantly, these topological nontrivial states have a large band gap of about 42.5 meV (corresponding

*Corresponding author: zmw@sdu.edu.cn

to a temperature of 490.4 K). The possibility of switching between QSH and QAH states in a real material via electrical gating (electron doping) offers not only an intriguing platform for the fundamental study of quantum phase transitions but for a different device paradigm as well, by interfacing between the QSH and QAH states.

II. METHOD AND COMPUTATIONAL DETAILS

Our first-principles calculations were performed using the Vienna *ab initio* simulation package (VASP) [24,25]. For the electron-electron interaction, we employed a generalized gradient approximation (GGA) in the form of that proposed by Perdew-Burke-Ernzerhof (PBE) [26]. The electron-ion interaction was described by projector-augmented-wave (PAW) potentials [27]. The vacuum region of about 15 Å was set up along the z direction to avoid mirror interactions between neighboring images. Structural optimizations were performed using a conjugate gradient (CG) method until the remanent force on each atom was less than 0.005 eV/Å. A plane-wave energy cutoff of 500 eV was used on a $1\times1\times1$ Monkhorst-Pack sampling in the Brillouin zone (BZ) for CG calculations and on a $3\times3\times1$ sampling for total energy calculations. The electron-doping effect was simulated by adding additional electrons to the lattice with a homogeneous background charge of opposite sign, as done before for other proposed OTIs [17,28]. Electron spin polarization was considered in all calculations.

III. RESULTS AND DISCUSSION

A triphenylene hexathiol (HTT) molecule contains a triphenylene core and three chelating dithiolenes. The structural symmetry of the core and the feasibility of covalent metal-dithiolene links make it an ideal molecular building block in the syntheses of porous polymer organometallic frameworks, such as the HTT-Pt synthesized by directly reacting HTT with $PtCl_2$ [29]. In HTT-Pt, each HTT unit coordinates with three Pt atoms, forming a structurally perfect kagome lattice pattern as denoted by dashed lines in Fig. 1(a). Structural relaxation showed that the planar configuration and sixfold symmetry are both well preserved, which can be attributed to the fully conjugate features of the framework. The optimized lattice constant of the HTT-Pt monolayer is $a = 23.61$ Å, slightly longer than the experimental value (23.29 Å) measured from a staggered stacking among the neighboring HTT-Pt sheets, whereas the length of the Pt-S distance (2.27 Å) is shorter than the experimental value (2.36 Å). The lengths of the C-S and C-H bonds are 1.72 and 1.09 Å, respectively. The covalent bonds between carbon atoms vary from 1.40 to 1.46 Å in length, very close to that in graphene (1.42 Å). The pristine HTT-Pt is a normal insulator with a trivial band gap of 0.313 eV at the Γ point, as indicated by our density functional theory (DFT) calculations, whose band structures without SOC and the projected electronic density of states (PDOS) onto different atoms are plotted in Fig. 1(b). As we can see, typical kagome bands comprising one flat band above two Dirac bands are located at the conduction band region. The PDOS clearly shows that these kagome bands come mainly from the platinum and sulfur atoms.

We tried to move the Fermi level (E_F) upward to the kagome band region by electron doping (or gate voltage). Our first-principles calculations indicate that at a doping concentration of 4.14×10^{13} cm^{-2} (two additional electrons in one unit cell), the Fermi level is located exactly at the Dirac point, with the kagome bands remaining intact, as shown in Fig. 2(a). Electron doping slightly enlarged the lattice constant by about 0.4%. Both time-reversal symmetry $[E(k,\uparrow) = E(-k,\downarrow)]$ and space-reversal symmetry $[E(k,\uparrow) = E(-k,\uparrow)]$ are well preserved, leading to the spin-degenerated energy dispersion [30,31]. Such a doping level is experimentally achievable based on the current techniques [11]. Taking the SOC into account, our first-principles calculations demonstrate that the degeneracies of the two Dirac bands at the K point, and of the upper Dirac band and flat band at the Γ point are lifted, leading to energy gaps of $\Delta_1 = 42.6$ and $\Delta_2 = 54.5$ meV,

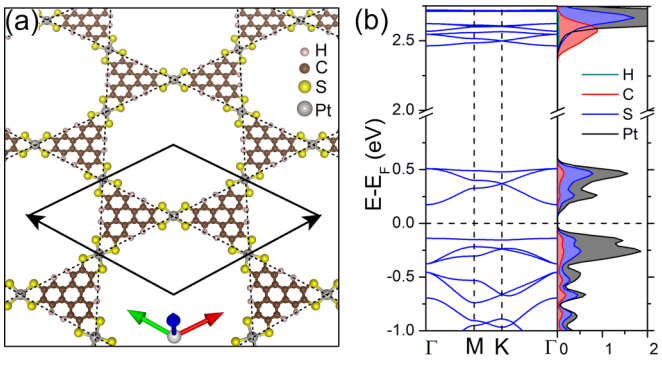

FIG. 1. (a) Schematic representation of HTT-Pt with the unit cells indicated by solid lines and the kagome lattice pattern by dashed lines. (b) Band structure and PDOS of the pristine HTT-Pt. The energy at the Fermi level was set to zero.

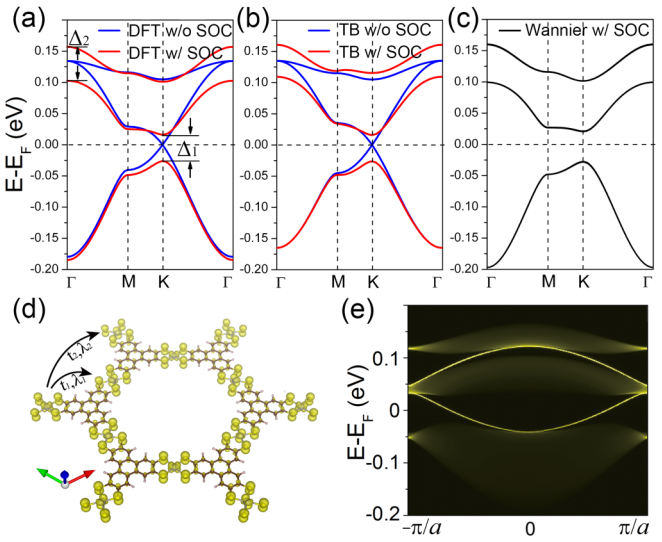

FIG. 2. The band structures of HTT-Pt calculated from (a) first principles (DFT), (b) TB models, and (c) MLWFs without and with SOC at a doping concentration of 4.14×10^{13} cm^{-2}. (d) The partial charge density isosurfaces decomposed to the kagome bands with an isosurface value of 0.002 Å^{-3}. The NN and NNN interactions of the single-orbital TB model are marked. (e) The semi-infinite Dirac edge states within the SOC gaps.

respectively, as shown in Fig. 2(a). We attribute such a large SOC gap to the strong SOC strength of the heavy Pt atom [32].

The kagome band structures of the electron-doped HTT-Pt can be reproduced by using a single-orbital tight-binding (TB) Hamiltonian (H_{TB}) in combination with an intrinsic SOC term (H_{SOC}): $H = H_{TB} + H_{SOC}$. It is interesting to see that an ideal kagome lattice pattern can be extracted from the partial charge density isosurfaces projected to the kagome bands [see Fig. 2(d)]. The TB Hamiltonian of the kagome lattice involves the nearest-neighbor (NN) and next-nearest-neighbor (NNN) interactions [33] and can be expressed in reciprocal space as follows:

$$H_{TB} = \begin{pmatrix} \varepsilon_{on} & 2t_1\cos k_1 & 2t_1\cos k_2 \\ 2t_1\cos k_1 & \varepsilon_{on} & 2t_1\cos k_3 \\ 2t_1\cos k_2 & 2t_1\cos k_3 & \varepsilon_{on} \end{pmatrix} + \begin{pmatrix} 0 & 2t_2\cos(k_2+k_3) & 2t_2\cos(k_3-k_1) \\ 2t_2\cos(k_2+k_3) & 0 & 2t_2\cos(k_1+k_2) \\ 2t_2\cos(k_3+k_1) & 2t_2\cos(k_1+k_2) & 0 \end{pmatrix}, \quad (1)$$

where the wave vectors are $k_1 = k_x a/2$, $k_2 = k_x a/4 + \sqrt{3}k_y a/4$, and $k_3 = -k_x a/4 + \sqrt{3}k_y a/4$. ε_{on} is the on-site energy. t_1 and t_2 correspond to the NN and NNN hopping parameters [see Fig. 2(d)], respectively. The SOC term is:

$$H_{SOC} = \pm i2\lambda_1 \begin{pmatrix} 0 & \cos k_1 & -\cos k_2 \\ -\cos k_1 & 0 & \cos k_3 \\ \cos k_2 & -\cos k_3 & 0 \end{pmatrix} \pm i2\lambda_2 \begin{pmatrix} 0 & -\cos(k_2+k_3) & \cos(k_3-k_1) \\ \cos(k_2+k_3) & 0 & -\cos(k_1+k_2) \\ -\cos(k_3+k_1) & \cos(k_1+k_2) & 0 \end{pmatrix}. \quad (2)$$

The two parameters (λ_1,λ_2) correspond to the NN and NNN SOC [see Fig. 2(d)], respectively, and $+/-$ refers to the spin-up/spin-down channels that are degenerated in energy for the TRS-protected QSH insulators. Using the following optimal parameters— $\varepsilon_{on} = 35.0$ meV, $t_1 = -45.0$ meV, $t_2 = -5.0$ meV, $\lambda_1 = 6.0$ meV, and $\lambda_2 = 1.6$ meV—the kagome bands of the electron-doped HTT-Pt without and with SOC are well reproduced, respectively, as shown in Fig. 2(b). This confirms that the band gap opened at the Dirac point arises from the intrinsic SOC of the heavy Pt atom.

The topological nontriviality of the band gap can be determined using the parity criteria proposed by Fu and Kane [34]. In this strategy, the Z_2 topological index ν is defined as

$$(-1)^{\nu} = \prod_i \delta_i \quad \text{with} \quad \delta_i = \prod_{m=1}^{N} \xi_{2m}(\Gamma_i) \quad (3)$$

for 2N occupied bands. $\xi_{2m}(\Gamma_i) = \pm 1$ is the parity eigenvalue of the $2m$th occupied energy band at the time-reversal invariant momentum Γ_i. This method has been widely used to confirm the topological aspects of TIs [35,36]. The calculated δ_i of the HTT-Pt are (+), (−), (−), and (−) at the four time-reversal momenta (0,0), ($\frac{1}{2}$,0), (0, $\frac{1}{2}$), and ($-\frac{1}{2}$, $\frac{1}{2}$), leading to a nonzero Z_2 topological invariant of $\nu = 1$. This implies the topological nontriviality of the electron-doped HTT-Pt.

Since the existence of topological edge states is an important signature of the 2D TIs, we calculated the edge states of the HTT-Pt lattice by employing the WANNIER90 package [37]. We first established maximally localized Wannier functions (MLWFs) using the *s* and *p* orbitals of S atom and the *d* orbitals of the Pt atom as an initial guess for the unitary transformations. The band structure fitted using Wannier interpolation within the energy window ($E_F - 0.2, E_F + 0.2$) eV is plotted in Fig. 2(c), which reproduced well the DFT bands. Based on a recursive strategy [38], the edge Green's function of the *semi*-infinite lattice was constructed from the MLWFs. The local density of states (LDOS) of the edges calculated from the Green's function is plotted in Fig. 2(e). From this figure, we can see that the bulk states are connected by the topologically nontrivial edge states, which is a feature of QSH insulators. More importantly, the bulk SOC band gap is well separated from other bands and thus implementable for achieving the QSH effect at room temperature.

We then further increased the doping concentration to 8.28×10^{13} cm^{-2} (four electrons in one unit cell), which is experimentally accessible using the current techniques [11]. The HTT-Pt framework is stable at this doping level, because the lattice constant is stretched only by less than 1%. The Fermi level was expected to be shifted upward into the region between the flat band and the upper Dirac band, provided that the kagome bands remain intact. However, our DFT calculations showed that the TRS is broken at this doping level, leading to spontaneous electron spin-polarization with a magnetic moment of 2.0 μ_B per unit cell. The spin-polarized electron density calculated from the charge density difference between spin-up and spin-down channels at ferromagnetic (FM) ordering, $\delta\rho = \rho_\uparrow - \rho_\downarrow$, is plotted in Fig. 3(a). Each S or Pt atom has a magnetic moment of 0.0924 or 0.1507 μ_B, which contribute to the magnetic moment of approximately 55.44% or 22.61% after considering the number of each atomic species per unit cell, respectively. Ground state analysis demonstrates that the FM ordering is energetically more favorable than the "antiferromagnetic" one (AFM) [see Fig. 3(b)] by about 26.2 meV and the spin-unpolarized one by about 36.7 meV per unit cell. The electron spin polarization is related to the instability of the partially filled flat band. Owing to the overlap between the flat band and Dirac bands, as shown in Fig. 1(b), electrons begin to occupy the flat band as the Fermi level is moved upward to this region. The instability of the partially filled flat band leads to spontaneous electron spin polarization to reduce the energy of the system [19,39]. As a consequence, the spin degeneracy of the kagome bands is lifted. The kagome bands of one spin channel (up spin) are fully occupied by electrons, while only one Dirac band of the other channel (down spin) is filled. The Fermi level is located right at the Dirac point of the spin-down channel, as shown in Fig. 3(c). Spin-polarization Dirac cones have been reported in many systems [39,40], however, the electron-doping-induced spin-polarized Dirac cones have not been reported to date. This offers a promising approach for tuning the magnetic properties via electric field.

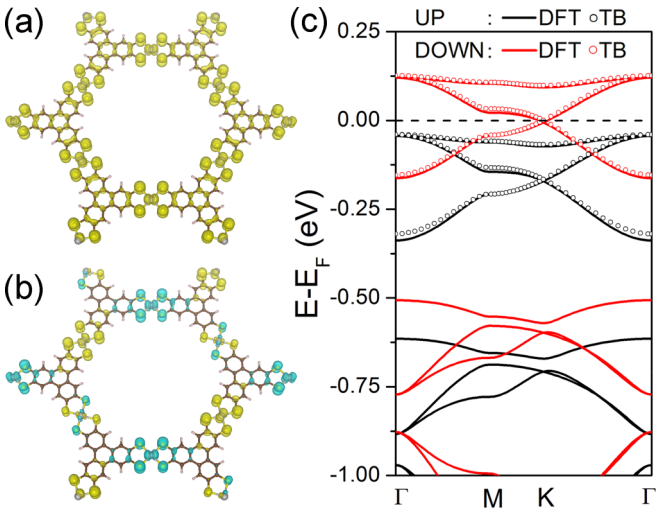

FIG. 3. The spin-polarized electron density ($\delta\rho$) at (a) FM and (b) AFM ordering with an isosurface value of 0.001 Å^{-3}. (c) A comparison between the band structures of the heavy electron-doped HTT-Pt calculated from first principles (DFT) and a spin-polarized TB model without SOC.

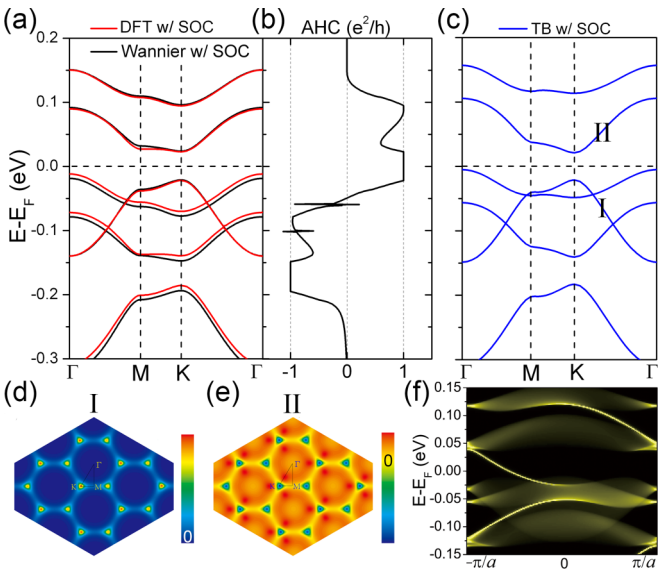

FIG. 4. (a) A comparison between the band structures of the heavy electron-doped HTT-Pt calculated from first principles (DFT) and MLWFs with SOC. (b) The calculated AHC and (f) the semi-infinite Dirac edge states near the Fermi level based on MLWFs. (c) TB band structure calculated from the spin-polarized Hamiltonian within the intrinsic SOC term. (d) and (e) Berry curvatures in reciprocal space for bands I and II marked in (c).

The electron-doping-induced spin polarization can also be reproduced by using the above TB Hamiltonian in combination with an exchange field (M) [18]. Without SOC, the spin-polarized Hamiltonian is

$$H_{\text{spin}} = \begin{pmatrix} 1 & 0 \\ 0 & 1 \end{pmatrix} \otimes H_0 - M \sum_{i,\alpha,\beta} c^{+}_{i\alpha} s^{z}_{\alpha\beta} c_{i\beta}. \qquad (4)$$

Here, $c^{+}_{i\alpha}$ and $c_{i\alpha}$ are creation and annihilation operators, respectively, for an electron with spin α on site i. Diagonalizing the above Hamiltonian in reciprocal space, we obtain the TB band structures shown in Fig. 3(c), which reproduce well the spin-polarized kagome bands given by DFT calculations with the optimal parameters of $\varepsilon_{\text{on}} = -50.0$ meV, $t_1 = -42.0$ meV, $t_2 = -4.7$ meV, and $M = -83.0$ meV.

Taking SOC into account, our DFT calculations revealed a band gap of 42.5 meV opened at the Fermi level, as shown in Fig. 4(a). Based on the MLWFs constructed from the initial guess similar to Fig. 2(c) within the energy window $(E_F - 0.4, E_F + 0.2)$ eV, the SOC gap can be well fitted by employing Wannier interpolation [see Fig. 4(a)]. The topological nontriviality of the heavy electron-doped HTT-Pt can then be evidenced by the Chern number (C) of the spin-polarized bands calculated using the Kubo formula [41,42]. A similar strategy has been successfully adopted in confirming the QAH states in a well-designed graphene nanomesh [43]. The calculated anomalous Hall conductivity (AHC) as a function of the electron filling is presented in Fig. 4(b), which shows that the AHC develops plateaus at a value of $e^2/\hbar$ at the Fermi level, indicating that the HTT-Pt doped with four electrons per unit cell is a Chern TI characterized by a finite Chern number ($C = 1$).

The SOC gap can also be reproduced by introducing the intrinsic SOC term (H_{SOC}) into the spin-polarized Hamiltonian (H_{spin}) with the SOC parameters $\lambda_1 = 6.0$ meV and $\lambda_2 = 1.6$ meV [see Fig. 4(c)], confirming that the appearance of the band gap is due to intrinsic SOC. The Berry curvatures of the two Dirac bands [bands I and II in Fig. 4(c)] calculated from the single-orbital TB Hamiltonian are shown in Figs. 4(d) and 4(e). It is clear that the Berry curvature of band I resides mainly around the K points with positive values, while that of band II is more dispersive in momentum space with positive and negative values, coinciding with the above Chern number calculation.

To further confirm the topological nontriviality of the system, we calculated the edge states of the spin-polarized HTT-Pt using the edge Green's function strategy. The LDOS of the edges shown in Fig. 4(f) exhibits clear features of TRS breakage, i.e., only one channel connects the bulk states. The large SOC bulk band gap and topologically nontrivial edge states in the heavy electron-doped HTT-Pt are promising for achieving a QAH effect at high temperatures. Additionally, the electron-doping-induced multiple quantum states (QSH and QAH) in HTT-Pt present the possibility of designing a QSH/QAH interface in a real material [44].

Notably, compared with the large bulk band gaps predicted in inorganic TIs (0.74–1.08 eV) [45,46], the bulk gaps of OTIs are usually very small, 2.4–22.7 meV, partly due to the weak SOC of the transition metal atoms. The incorporation of Pt atoms into the *trans*-Pt-(NH)S framework has been shown to improve the SOC gap to ~50 meV of the QSH state [32]. Similarly, large SOC gaps are predicted here in the real experimental sample, HTT-Pt, and especially the 42.5 meV gap for the QAH state. Additionally, breaking TRS in Z_2 TIs was commonly achieved by doping with magnetic atoms [3,47] or by introducing proximity coupling with an antiferromagnetic insulator [48,49]. Our work offers an alternative approach of inducing ferromagnetism in TIs that is reversible.

IV. CONCLUSIONS

In summary, we demonstrate from first principles that already synthesized HTT-Pt can undergo a reversible QSH-QAH transition through electron doping, exhibiting tunable topological properties. At the low electron doping concentration of $4.14\times10^{13}\,\mathrm{cm}^{-2}$, the HTT-Pt is a QSH insulator characterized by a nonzero Z_2 topological invariant. At a higher electron doping level, $8.28\times10^{13}\,\mathrm{cm}^{-2}$, TRS is broken, leading to a robust QAH state with the Chern number $C = 1$. Also, the topologically nontrivial bulk band gap is as large as 42.5 meV (~490.4 K), implying that the critical temperatures of realizing QSH and QAH effects are above room temperature. The possibility of switching between two QSH and QAH states in a real material via electrical gating (doping) offers not only an intriguing platform for the fundamental study of quantum phase transitions, but also different device paradigm by interfacing between a QSH and QAH state.

ACKNOWLEDGMENTS

This work is supported by the National Basic Research Program of China (No.2012CB932302), the National Natural Science Foundation of China (No. 21433006), the 111 Project (No. B13029), and the National Super Computing Centre, Jinan, China. F.L. acknowledges support from the Office of Basic Energy Sciences of the U.S. Department of Energy (Grant No. DE-FG02-04ER46148).

[1] C. L. Kane and E. J. Mele, Phys. Rev. Lett. **95**, 146802 (2005).
[2] F. D. M. Haldane, Phys. Rev. Lett. **61**, 2015 (1988).
[3] J. Ding, Z. Qiao, W. Feng, Y. Yao, and Q. Niu, Phys. Rev. B **84**, 195444 (2011).
[4] H. Jiang, Z. Qiao, H. Liu, and Q. Niu, Phys. Rev. B **85**, 045445 (2012).
[5] K. S. Novoselov, A. K. Geim, S. V. Morozov, D. Jiang, Y. Zhang, S. V. Dubonos, I. V. Grigorieva, and A. A. Firsov, Science **306**, 666 (2004).
[6] X. Du, I. Skachko, F. Duerr, A. Luican, and E. Y. Andrei, Nature (London) **462**, 192 (2009).
[7] K. I. Bolotin, F. Ghahari, M. D. Shulman, H. L. Stormer, and P. Kim, Nature (London) **462**, 196 (2009).
[8] A. Das *et al.*, Nat. Nanotechnol. **3**, 210 (2008).
[9] J. Yan, T. Villarson, E. A. Henriksen, P. Kim, and A. Pinczuk, Phys. Rev. B **80**, 241417(R) (2009).
[10] K. F. Mak, C. H. Lui, J. Shan, and T. F. Heinz, Phys. Rev. Lett. **102**, 256405 (2009).
[11] J. Ye, M. F. Craciun, M. Koshino, S. Russo, S. Inoue, H. Yuan, H. Shimotani, A. F. Morpurgo, and Y. Iwasa, Proc. Natl. Acad. Sci. USA **108**, 13002 (2011).
[12] J. H. Cho, J. Lee, Y. He, B. S. Kim, T. P. Lodge, and C. D. Frisbie, Adv. Mater. **20**, 686 (2008).
[13] A. S. Dhoot, C. Israel, X. Moya, N. D. Mathur, and R. H. Friend, Phys. Rev. Lett. **102**, 136402 (2009).
[14] J. T. Ye, S. Inoue, K. Kobayashi, Y. Kasahara, H. T. Yuan, H. Shimotani, and Y. Iwasa, Nat. Mater. **9**, 125 (2010).
[15] K. Ueno, S. Nakamura, H. Shimotani, A. Ohtomo, N. Kimura, T. Nojima, H. Aoki, Y. Iwasa, and M. Kawasaki, Nat. Mater. **7**, 855 (2008).
[16] B. Yan, M. Jansen, and C. Felser, Nat. Phys. **9**, 709 (2013).
[17] Z. F. Wang, Z. Liu, and F. Liu, Nat. Commun. **4**, 1471 (2013).
[18] Z. F. Wang, Z. Liu, and F. Liu, Phys. Rev. Lett. **110**, 196801 (2013).
[19] Z. Liu, Z.-F. Wang, J.-W. Mei, Y.-S. Wu, and F. Liu, Phys. Rev. Lett. **110**, 106804 (2013).
[20] T. Kambe *et al.*, J. Am. Chem. Soc. **135**, 2462 (2013).
[21] M. Zhao, A. Wang, and X. Zhang, Nanoscale **5**, 10404 (2013).
[22] D. Sheberla, L. Sun, M. A. Blood-Forsythe, S. Er, C. R. Wade, C. K. Brozek, A. Aspuru-Guzik, and M. Dinca, J. Am. Chem. Soc. **136**, 8859 (2014).
[23] B. Zhao, J. Zhang, W. Feng, Y. Yao, and Z. Yang, Phys. Rev. B **90**, 201403 (2014).
[24] G. Kresse and J. Furthmüller, Phys. Rev. B **54**, 11169 (1996).
[25] G. Kresse and J. Hafner, Phys. Rev. B **48**, 13115 (1993).
[26] J. P. Perdew, K. Burke, and M. Ernzerhof, Phys. Rev. Lett. **77**, 3865 (1996).
[27] G. Kresse and D. Joubert, Phys. Rev. B **59**, 1758 (1999).
[28] Z. F. Wang, N. Su, and F. Liu, Nano Lett. **13**, 2842 (2013).
[29] J. Cui and Z. Xu, Chem. Commun. (Cambridge, UK) **50**, 3986 (2014).
[30] T. Hirahara, T. Nagao, I. Matsuda, G. Bihlmayer, E. V. Chulkov, Y. M. Koroteev, P. M. Echenique, M. Saito, and S. Hasegawa, Phys. Rev. Lett. **97**, 146803 (2006).
[31] Y. Xia *et al.*, Nat. Phys. **5**, 398 (2009).
[32] Q. Zhou, J. Wang, T. S. Chwee, G. Wu, X. Wang, Q. Ye, J. Xu, and S. W. Yang, Nanoscale **7**, 727 (2015).
[33] E. Tang, J.-W. Mei, and X.-G. Wen, Phys. Rev. Lett. **106**, 236802 (2011).
[34] L. Fu and C. L. Kane, Phys. Rev. B **79**, 161408(R) (2009).
[35] M. Zhao, W. Dong, and A. Wang, Sci. Rep. **3**, 3532 (2013).
[36] A. Wang, X. Zhang, and M. Zhao, Nanoscale **6**, 11157 (2014).
[37] A. A. Mostofi, J. R. Yates, Y.-S. Lee, I. Souza, D. Vanderbilt, and N. Marzari, Comput. Phys. Commun. **178**, 685 (2008).
[38] M. P. Lopez Sancho, J. M. Lopez Sancho, J. M. L. Sancho, and J. Rubio, J. Phys. F: Met. Phys. **15**, 851 (1985).
[39] X. Zhang, A. Wang, and M. Zhao, Carbon **84**, 1 (2015).
[40] Y. Ma, Y. Dai, X. Li, Q. Sun, and B. Huang, Carbon **73**, 382 (2014).
[41] D. J. Thouless, M. Kohmoto, M. P. Nightingale, and M. den Nijs, Phys. Rev. Lett. **49**, 405 (1982).
[42] Y. Yao, L. Kleinman, A. H. MacDonald, J. Sinova, T. Jungwirth, D.-s. Wang, E. Wang, and Q. Niu, Phys. Rev. Lett. **92**, 037204 (2004).
[43] X. Zhang and M. Zhao, R. Soc. Chem. Adv. **5**, 9875 (2015).
[44] H. Huang, Z. Wang, N. Luo, Z. Liu, R. Lü, J. Wu, and W. Duan, Phys. Rev. B **92**, 075138 (2015).
[45] L. Li, X. Zhang, X. Chen, and M. Zhao, Nano Lett. **15**, 1296 (2015).
[46] C.-C. Liu, S. Guan, Z. Song, S. A. Yang, J. Yang, and Y. Yao, Phys. Rev. B **90**, 085431 (2014).
[47] X.-L. Zhang, L.-F. Liu, and W.-M. Liu, Sci. Rep. **3**, 2908 (2013).
[48] Z. Qiao, W. Ren, H. Chen, L. Bellaiche, Z. Zhang, A. H. MacDonald, and Q. Niu, Phys. Rev. Lett. **112**, 116404 (2014).
[49] J. Zhang, B. Zhao, Y. Yao, and Z. Yang, Sci. Rep. **5**, 10629 (2015).